



Identification of key candidate genes and pathways revealing the protective effect of liraglutide on diabetic cardiac muscle by integrated bioinformatics analysis

Ying Dong¹, Shi Yan², Guo-Yan Li¹, Min-Nan Wang¹, Lei Leng¹, Qiang Li¹

¹Department of Endocrinology and Metabolic Disease, The 2nd Affiliated Hospital of Harbin Medical University, Harbin 150081, China; ²The Fourth Medical Ward, The Tumor Hospital of Harbin Medical University, Harbin 150081, China

Contributions: (I) Conception and design: Y Dong, Q Li; (II) Administrative support: Y Dong, S Yan; (III) Provision of study materials: GY Li, MN Wang, L Leng, Y Dong; (IV) Collection and assembly of data: Y Dong, Q Li; (V) Data analysis and interpretation: GY Li, MN Wang, L Leng, Y Dong; (VI) Manuscript writing: All authors; (VII) Final approval of manuscript: All authors.

Correspondence to: Qiang Li. Department of Endocrinology and Metabolic Disease, The 2nd Affiliated Hospital of Harbin Medical University, Harbin 150081, China. Email: qiangli126@126.com.

Background: Diabetes mellitus is becoming a significant health problem with the International Diabetes Federation (IDF) expecting a startling 642 million diabetes patients by 2040. Liraglutide, a glucagon-like peptide-1 (GLP-1) analog, is reported to protect against diabetic cardiomyopathy by binding to the receptor, GLP-1R. However, the underlying mechanism has yet to be clarified. This study aimed to investigate the underlying mechanisms and the effects of liraglutide on diabetic patient's cardiac muscles.

Methods: GSE102194 genetic expression profiles were extracted from the Gene Expression Omnibus (GEO) database. The gene ontology (GO) and Kyoto Encyclopedia of Genes and Genomes pathway (KEGG) enrichment analyses were carried out. Next, Cytoscape software was used to construct the protein-protein interaction (PPI) network of the differentially expressed genes (DEGs). DEGs were mapped onto a protein-protein interaction (PPI) network that comprised 249 nodes and 776 edges.

Results: A total of 520 DEGs were discovered, including 159 down-regulated genes and 361 up-regulated genes. DEGs that were upregulated were notably enriched in biological processes (BP) such as muscle system process, muscle system process, muscle structure development and anatomical structure morphogenesis while DEGs that were downregulated were rich in detection of chemical stimulus and neurological system process. KEGG pathway analysis showed the up-regulated DEGs were enriched in adrenergic signaling for cardiomyocytes, dopaminergic synapse, and circadian entrainment, while the down-regulated DEGs were enriched for factory transduction in 249 of the 520 tested samples. The modular analysis identified 4 modules that participated in some pathways associated with cardiac muscle contraction, hypertrophic cardiomyopathy (HCM), and MAPK signaling pathway.

Conclusions: Our data showed that Glp-1 could decrease the protein expression of p38, JNK, ERK1/2, and MARS proteins induced by high glucose (22 mM, 72 h). This study highlights the potential physiological processes that take place in diabetic cardiac muscles exposed to liraglutide. Our findings elucidated the regulatory network in diabetic cardiomyopathy and might provide a novel diagnostic and therapeutic target for diabetic cardiomyopathy.

Keywords: Liraglutide; bioinformatics analysis; network modules; microarray; differentially expressed genes (DEGs)

Submitted Sep 04, 2019. Accepted for publication Jan 03, 2020.

doi: 10.21037/atm.2020.01.94

View this article at: <http://dx.doi.org/10.21037/atm.2020.01.94>

Introduction

Diabetes mellitus is becoming a major health problem as the International Diabetes Federation (IDF) expects an astounding 642 million diabetes patients by 2040 (1). This chronic metabolic disease causes a series of serious long-term complications affecting the cardiovascular system, peripheral vascular system, central nervous system, and renal function (2). Diabetic cardiomyopathy, among these, exists independently of macro- and micro-coronary artery diseases and other cardiovascular diseases, and presents a high risk of cardiovascular morbidity and mortality (3).

The major pathological manifestations of diabetic cardiomyopathy include hypertrophy, ventricular dilatation, and compromised contractile function, which may be attributed to apoptosis and interstitial fibrosis, leading to ventricular remodeling (1). Previous studies from our lab and others have depicted a few pathophysiological factors that are involved in the onset and development of diabetic cardiomyopathy, including glucose and lipid toxicity, inflammation, oxidative stress, mitochondrial injury, interstitial fibrosis, apoptosis, and dysregulated autophagy (2,3).

Little is known about the physiological process that underlies the progression of diabetic cardiomyopathy, which prohibits adequate treatment. As such, a deeper understanding of the specific processes that govern cell apoptosis and proliferation, as well as the progression of diabetic cardiomyopathy, are crucial for the invention of better therapeutic and diagnostic modalities.

Liraglutide is a glucagon-like peptide-1 (GLP-1) analog that binds to the GLP-1R receptor and has been shown to be abundantly expressed by RGC-5 cells (4). A GLP-1 homolog, exendin [9–39], is 53% similar in sequence homology and is commonly utilized as a GLP-1 receptor antagonist in experimental studies (5). Zhang *et al.* reported Glp1r expression on retinal ganglion cells and investigated the GLP-1 protective mechanisms against hyperglycaemic conditions (6). The diabetic retina in the early stages of DR is protected by GLP-1 (7). Liraglutide enhances a systemic glycaemic reduction while providing multiple protective effects against diabetic complications (8,9). Despite previous research, the specific role of GLP-1 on diabetic cardiomyopathy has yet to be investigated. Therefore, the current study used the microarray dataset, GSE102194 which was extracted from the NCBI-Gene Expression Omnibus database (NCBI-GEO) (<https://www.ncbi.nlm.nih.gov/geo>).

The sample size included cardiac muscle samples of 3 liraglutide-treated rats and 3 untreated controls. Differentially expressed genes (DEGs) were identified and used to perform the Gene Ontology and pathway enrichment analyses using the DAVID online tool. Protein-protein interaction (PPI) networks (<http://string-db.org>) and modular analysis were constructed to discern hub genes. We also found that these modules were associated with cardiac muscle contraction, hypertrophic cardiomyopathy (HCM), and MAPK signaling pathway. We also confirmed that Glp-1 increased H9c2 cell growth after treatment with a high volume of glucose (22 mM, 72 h) using CCK-8 assays. Glp-1 attenuated high glucose-induced cell apoptosis accompanied by a decrease in the level of proinflammatory cytokines (IL-1, IL-1 β , and TNF- α) as confirmed by the ELASE kit. Glp-1 also decreased the expression of p38, JNK, ERK1/2, and MARS proteins induced by HG. DEG identification, along with the respective enriched biological pathways and functions, may provide immense insight into the mechanism of liraglutide-protected diabetic cardiomyopathy.

Methods

Microarray data information

GSE102194 gene expression profiles were extracted from the GEO database. GSE102194, which was based on GPL17117 platform Affymetrix Rat Gene 2.0 ST Array) (10). The GSE102194 cohort comprised 6 samples, including the cardiac muscle of 3 liraglutide-treated rats and that of 3 controls.

DEG identification

Raw data files were downloaded in TXT file formats (Affymetrix platform), with subsequent analyses completed on the GEO2R software. Hierarchical clustering analysis was applied to group the data into 2 similar expression patterns of liraglutide-treated and control rat cardiac muscle. Principal component analysis (PCA) in GeneSpring was used to determine probe quality control. The cutoff criterion for statistically significant DEGs was defined as (logFC) >1.

Functional enrichment analysis of DEGs

Candidate DEGs enriched pathways and functions were

discerned using the DAVID tool, a freely available online tool that allows gene visualization and annotation as well as integrated discovery function, allowing for a holistic interpretation of the biological function of any one gene (<https://david.ncifcrf.gov/>) (11). Gene ontology analysis (GO) is a commonly used means of gene and gene product annotation; it is also able to determine the defining biological characteristics of high-throughput genome or transcriptome data (12). The Kyoto Encyclopedia of Genes and Genomes (KEGG) (<http://www.genome.jp/>) is a database of genetic functions that links both functional and genomic information (13). Both a $P < 0.01$ and $FDR < 0.05$ were taken to indicate statistical significance.

Integration of protein-protein interaction (PPI) network and modular analysis

DEGs were mapped onto the STRING (Search Tool for the Retrieval of Interacting Genes) database (version 9.0) to evaluate inter-DEG relationships via protein-protein interaction (PPI) information (<http://string-db.org>) (14). Protein interaction relationship networks were mapped using the Cytoscape software (15), which analyzed the relationship between candidate DEG encoding proteins in the cardiac muscle of liraglutide-treated rats. Node degree was calculated using the Network Analyzer plug-in, which involved determining the number of interconnections to sort out PPI hub genes. Molecular Complex Detection (MCODE) was utilized to filter PPI network modules on Cytoscape, selecting only modules with a node number of less than 4 and MCODE scores of more than 4. These nodules were then subjected to pathway and function enrichment analyses. $P < 0.01$ was determined as significantly different.

Cell culture and transfection

H9c2 cells were acquired from the Chinese Academy of Science, Shanghai Cell Bank and cultured in low glucose (5.5 mM) minimum essential medium (Gibco-Invitrogen, Grand Island, NY, USA) complemented with 10% heat-inactivated fetal bovine serum (FBS; Gibco BRL, Grand Island, NY, USA), 100 U/mL of penicillin, and 50 g/mL of streptomycin (Beyotime Institute of Biotechnology, China). The cells were placed in a humidified atmosphere containing 5% CO_2 at 37 °C.

To establish a high glucose- (HG-) induced stress model in H9c2 cells, D-glucose (Sinopharm Chemical Reagent Co. Ltd., Shanghai, China) was added in culture medium

to reach the final concentration of 22 mM glucose. The concentration of 5.5 mM glucose was used as the control group. A dose-dependent effect of propofol was evaluated by adding 5, 10, 20, and 40 μM of propofol to the cells.

Cell counting Kit (CCK)-8 assay

H9c2 cells were treated with Glp-1 and harvested into 96-well plates for 48 h. CCK8 (Dojindo Molecular Technologies, Japan) was tested at 450 nm by Multiskan Spectrum (Thermo Fisher, USA).

TUNEL assay

TUNEL assay was performed to examine the apoptosis of cells. Specifically, H9c2 cells were fixed with 4% formaldehyde and permeabilized with Cytonin. Streptavidin-fluorescein conjugate was applied to detect the biotinylated nucleotides. Fluorescein-stained cells were analyzed by fluorescence microscopy.

Flow cytometric analysis

The apoptotic assay was conducted using an Annexin V-FITC/PI Apoptosis Detection Kit (KeyGEN Biotech, Jiangsu, China). H9c2 cells were double-stained with Annexin V-FITC and propidium iodide (PI) and analyzed with flow cytometry (FACS-can, BD Biosciences). The relative ratio of early and terminal apoptotic cells was detected to calculate the apoptotic rate.

Enzyme-linked immunosorbent assay (ELISA) of IL-1 β , IL-6, and TNF- α

The relative levels of IL-6, IL-1 β , and TNF- α in our manuscript were evaluated by the ELISA kits (R&D Systems, USA) as their protocol.

Antibodies and western blot analysis

All proteins were obtained from H9c2 cells, cells were lysed with RIPA buffer, and 12.5% SDS-PAGE was used to separate the proteins. The proteins were transferred to a nitrocellulose membrane (Pall Corporation, USA) and blocked. Next, the blots were incubated with primary antibodies to p38; ERK1/2, JNK, and MRAS were bought from Cell Signaling Technology, USA. After washing and incubating with rabbit or mouse secondary antibodies (LI-COR Biosciences, USA), the blots were with the help of an Infrared Imaging System (LI-COR Biosciences, USA). The densities of bands were quantified using Odyssey 3.0 software. The blots were subjected to densitometry using

β -actin as an internal control. The densities of bands from each group were calculated.

Statistical analysis

Data were expressed as means \pm SD. Student's non-paired *t*-test or one-way analysis of variance (ANOVA) followed by Tukey's test were used to compare multiple groups. Differences were considered significant when $P < 0.05$. SPSS software (version 13.0; USA) was used to perform the analysis.

Results

DEG identification

DEGs were identified by separately analyzing microarray data from each chip with the GeneSpring software. Using ($\log_{2}FC$) > 1 as threshold cutoff point, 520 genes were highlighted. Of these, there were 159 down-regulated genes and 361 up-regulated genes in liraglutide-treated diabetic cardiac muscle in comparison to untreated diabetic cardiac muscle. A heat map of the 520 DEGs using data profile GSE102194 is shown in *Figure S1*.

GO term enrichment and KEGG pathway analyses

GO and pathway enrichment of DEGs were constructed with the DAVID online databases. The DEGs were categorized based on cellular components, biological processes, and molecular functions. In the biological process group, up-regulated genes were mainly enriched in the muscle system, development of muscle structure, and anatomical structure morphogenesis while the down-regulated DEGs were markedly enriched in biological processes, including the detection of chemical stimulus and neurological system process (*Figure 1A* and *Table 1*). GO cell component (CC) analysis also demonstrated significant enrichment of up-regulated DEGs in the sarcomere, contractile fiber, and neuron projection, and significant enrichment of down-regulated DEGs in the integral component of membrane (*Figure 1B* and *Table 2*). In addition, for molecular function (MF), the down-regulated DEGs were enriched in signaling receptor activity and transmembrane signaling receptor activity, while the upregulated DEGs were enriched in cytoskeletal protein and ion channel binding (*Figure 1C* and *Table 3*).

Table 4 and *Figure 1D* show the most significantly enriched pathways of the up-regulated and down-regulated DEGs as identified through KEGG analysis. The up-regulated DEGs were enriched in adrenergic signaling in cardiomyocytes, dopaminergic synapse and circadian entrainment, while down-regulated DEGs were enriched in factory transduction.

Identification of key candidate genes and pathways using protein-protein interaction network (PPI) and modular screening

With the STRING online database (Available online: <http://string-db.org>) and Cytoscape software, 249 DEGs of the 520 DEGs were mapped onto a PPI network, which included 776 edges and 249 nodes (*Figure 2A*). The top 10 hub nodes with higher degrees were further analyzed. These hub genes included Acta1, Actn2, Mapk12, Tnnc2, Actn3, Eno3, Myh1, Mylpf, Pgam2, and Pygm. Moreover, this network was further assessed with MCODE plug-ins. The top 4 modules from the PPI network were selected for functional annotation. Pathway annotation analysis demonstrated that Module 1 consisted of 17 nodes and 111 edges (*Figure 2B*, *Table 5*), which were primarily involved in tight junction, regulation of actin cytoskeleton, glycolysis/gluconeogenesis, and cardiac muscle contraction. Module 2 comprised 7 nodes and 15 edges (*Figure 2C*, *Table 5*), which were primarily involved with gap junction and phagosome. Module 3 and Module 4 (*Figure 2D,E*) were primarily involved in the MAPK signaling pathway and Synaptic vesicle cycle, respectively.

The effect of GLP-1 regulates the cell viability induced by high-glucose stress

To explore the role of Glp-1 in diabetic cardiac muscle. A diabetic cardiac muscle model was established by H9c2 cells. Treatment with different concentrations of glucose (5.5, 11.0, 22.0, and 44.0 mM) for 72 h. At the concentration of 22 mM, glucose significantly decreased the cell viability of H9c2 (*Figure S2*). Therefore, 22.0 mM glucose was used as a standard of high glucose-stress for further study. The effect of Glp-1 on the viability of H9c2 cells was measured by CCK8 assay. Compared to the high glucose (22 mM) group, Glp-1 increased H9c2 cell viability in a dose-dependent manner at the range of 5–20 nM. However, 40 nM of Glp-1 did not further improve cell viability during high-glucose

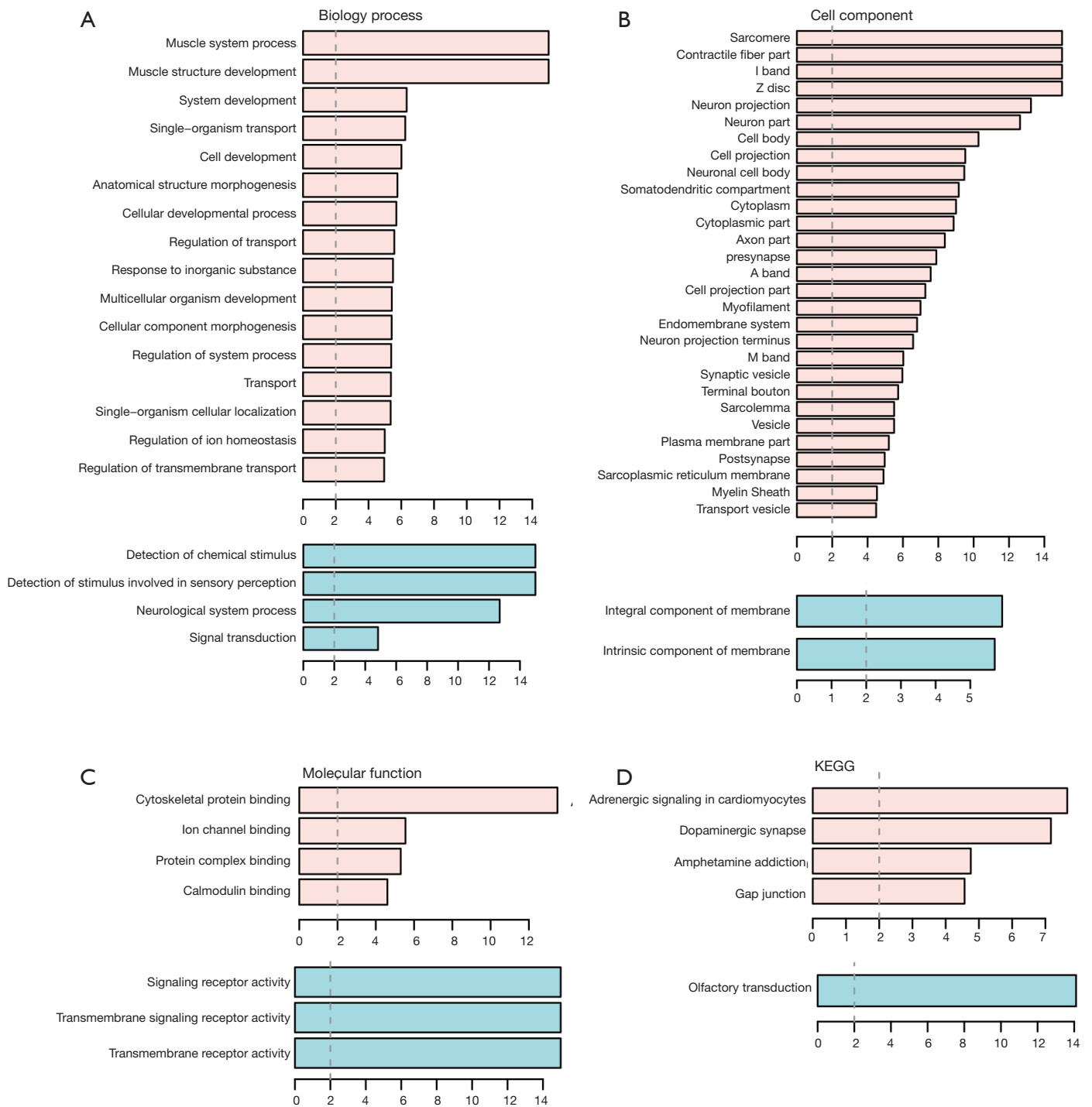


Figure 1 Significantly enriched (A) GO BP terms, (B) GO CC terms, (C) GO MF terms, and (D) KEGG pathway of DEGs. The X-axis represents the $-\log(P \text{ value})$.

Table 1 The significantly enriched GO BP terms of differentially expressed genes

Term	Count	P value	FDR
Up-regulated			
GO:0003012~muscle system process	42	3.75E-20	5.81E-17
GO:0061061~muscle structure development	50	7.47E-18	1.16E-14
GO:0048731~system development	126	4.69E-07	7.26E-04
GO:0044765~single-organism transport	96	5.72E-07	8.86E-04
GO:0048468~cell development	73	9.78E-07	0.001515
GO:0009653~anatomical structure morphogenesis	83	1.72E-06	0.002671
GO:0048869~cellular developmental process	114	2.00E-06	0.0031
GO:0051049~regulation of transport	63	2.67E-06	0.004138
GO:0010035~response to inorganic substance	32	3.20E-06	0.004966
GO:0007275~multicellular organism development	131	3.78E-06	0.00586
GO:0032989~cellular component morphogenesis	51	3.87E-06	0.005997
GO:0044057~regulation of system process	27	4.12E-06	0.006389
GO:0006810~transport	115	4.28E-06	0.006636
GO:1902580~single-organism cellular localization	40	4.46E-06	0.006906
GO:2000021~regulation of ion homeostasis	16	1.02E-05	0.015795
GO:0034762~regulation of transmembrane transport	23	1.10E-05	0.017111
Down-regulated			
GO:0009593~detection of chemical stimulus	41	3.00E-19	4.11E-16
GO:0050906~detection of stimulus involved in sensory perception	41	6.36E-19	8.72E-16
GO:0050877~neurological system process	42	2.04E-13	2.80E-10
GO:0007165~signal transduction	54	1.48E-05	0.020299

insult (*Figure 3A*).

GLP-1 decreases high-glucose-induced apoptosis in H9c2 Cells.

As shown in *Figure 3B*, after H9c2 cells were cultured with high glucose (22 mM, 72 h), the levels of IL-6, IL-1 β , and TNF- α were significantly increased in the media compared to the control group, whereas, pretreatment of GLP-1 at concentrations of 10 and 20 μ M significantly reduced IL-6, IL-1 β , and TNF- α expression. Compared to the 10 nM GLP-1 group, the 20 nM Glp-1 group further inhibited inflammatory cytokines. The number of apoptotic cells was labeled with TUNEL⁺. The result showed that the number of apoptotic H9c2 cells cultured with high glucose was

significantly increased compared to the control group, whereas pretreatment of GLP-1 at concentrations of 20 μ M significantly reduced the glucose-induced apoptotic cells (*Figure 3C,D*). Similar to our observations, the result of flow cytometric analysis showed the same pattern (*Figure 3E*). Our data suggest that GLP-1 can protect those H9c2 cells injured by high glucose-induced apoptosis.

GLP1 alleviated apoptosis induced by high-glucose stress in H9c2 Cells by MRAS /MAPK signaling pathway

Our previous results (*Table 5*) show that MRAS and MAPK signaling pathways might play an essential role in Glp-1-protected H9c2 cells that are injured by high glucose. Compared to the control group, high glucose significantly

Table 2 The significantly enriched GO CC terms of differentially expressed genes

Term	Count	P value	FDR
Up-regulated			
GO:0030017~sarcomere	41	8.75E-32	1.13E-28
GO:0044449~contractile fiber part	42	1.11E-31	1.43E-28
GO:0031674~I band	31	3.32E-25	4.27E-22
GO:0030018~Z disc	27	1.90E-21	2.44E-18
GO:0043005~neuron projection	63	5.74E-14	7.38E-11
GO:0097458~neuron part	72	2.38E-13	3.06E-10
GO:0044297~cell body	42	5.32E-11	6.83E-08
GO:0042995~cell projection	76	2.97E-10	3.82E-07
GO:0043025~neuronal cell body	38	3.38E-10	4.35E-07
GO:0036477~somatodendritic compartment	46	6.97E-10	8.96E-07
GO:0005737~cytoplasm	228	9.92E-10	1.27E-06
GO:0044444~cytoplasmic part	177	1.36E-09	1.75E-06
GO:0033267~axon part	25	4.27E-09	5.49E-06
GO:0098793~presynapse	25	1.29E-08	1.66E-05
GO:0031672~A band	10	2.70E-08	3.47E-05
GO:0044463~cell projection part	46	5.39E-08	6.93E-05
GO:0036379~myofilament	8	1.02E-07	1.31E-04
GO:0012505~endomembrane system	99	1.59E-07	2.04E-04
GO:0044306~neuron projection terminus	18	2.66E-07	3.42E-04
GO:0031430~M band	7	9.54E-07	0.001226
GO:0008021~synaptic vesicle	15	1.08E-06	0.001386
GO:0043195~terminal bouton	13	1.86E-06	0.002395
GO:0042383~sarcolemma	14	3.14E-06	0.004033
GO:0031982~vesicle	97	3.16E-06	0.004065
GO:0044459~plasma membrane part	70	6.27E-06	0.008055
GO:0098794~postsynapse	23	1.08E-05	0.013836
GO:0033017~sarcoplasmic reticulum membrane	7	1.26E-05	0.016165
GO:0043209~myelin sheath	15	2.95E-05	0.037942
GO:0030133~transport vesicle	18	3.28E-05	0.042101
Down-regulated			
GO:0016021~integral component of membrane	59	1.20E-06	0.001377
GO:0031224~intrinsic component of membrane	59	1.97E-06	0.002255

Table 3 The significantly enriched GO MF terms of differentially expressed genes

Term	Count	P value	FDR
Up-regulated			
GO:0008092~cytoskeletal protein binding	51	3.21E-14	3.84E-11
GO:0044325~ion channel binding	13	2.82E-06	0.003375
GO:0032403~protein complex binding	37	4.97E-06	0.005949
GO:0005516~calmodulin binding	13	2.49E-05	0.029743
Down-regulated			
GO:0038023~signaling receptor activity	52	1.09E-20	1.11E-17
GO:0004888~transmembrane signaling receptor activity	47	4.49E-17	4.54E-14
GO:0099600~transmembrane receptor activity	47	9.06E-17	1.11E-13

Table 4 The significantly enriched KEGG pathway of differentially expressed genes

Term	Count	P value	FDR
Up-regulated			
rno04261: adrenergic signaling in cardiomyocytes	16	2.20E-08	2.76E-05
rno04728: dopaminergic synapse	15	6.80E-08	8.53E-05
rno05031: amphetamine addiction	9	1.75E-05	0.021963
rno04540: gap junction	10	2.70E-05	0.033829
Down-regulated			
rno04740: olfactory transduction	37	7.92E-15	7.78E-12

decreased the protein levels of p38, JNK, EKR1/2, and MRAS. As expected, compared to the model group, the levels of p38, JNK, EKR1/2, and MRAS were increased with high glucose. Furthermore, GLP-1 could inhibit the expression of p38, JNK, EKR1/2, and MRAS induced by high glucose (*Figure 4A,B,C,D*).

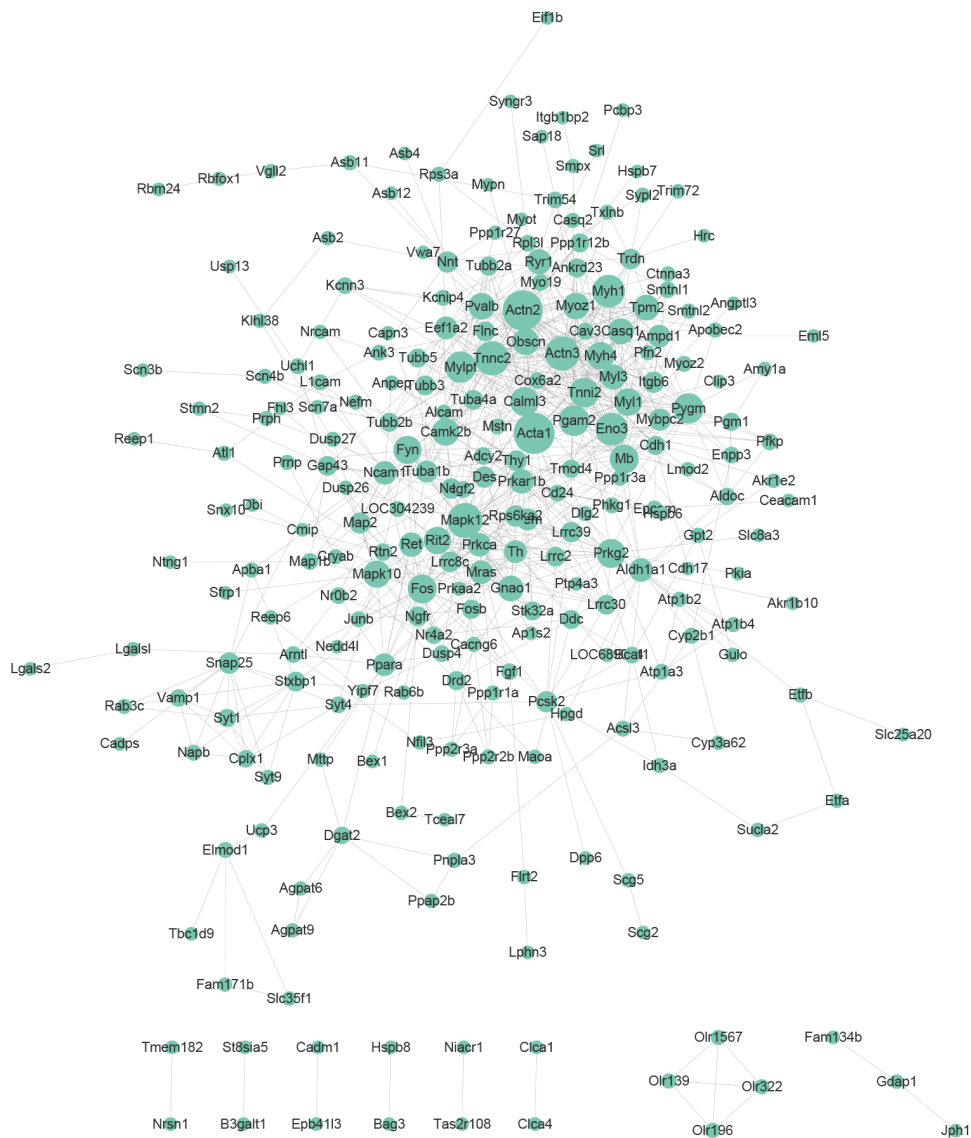
Discussion

Existing literature about the pathophysiological factors of diabetic cardiomyopathy either has only examined a single genetic event or generate results based on a single cohort (16). This lack of information has led towards the stunted progression of knowledge in this field, and indirectly, to the increased mortality and incidence of this deleterious condition. Liraglutide is a novel agent widely used in diabetes mellitus treatment (17). However, the understanding of the relationship between liraglutide and diabetic cardiomyopathy is unclear. Given that microarray

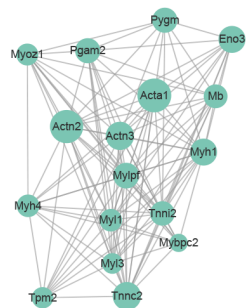
analysis and high throughput sequencing provides vast amounts of data on the human genome, these methods have been utilized as a means to predict likely therapeutic targets for liraglutide in diabetic cardiomyopathy treatment.

The current study used the GSE102194 dataset information and successfully extracted 520 DEGs (361 up-regulated and 159 down-regulated) from the cardiac muscle of liraglutide-treated diabetic rats and untreated controls. Functional annotation demonstrated that these DEGs were primarily associated with cardiomyocytes, dopaminergic synapses, and circadian entrainment. Through the construction of PPIs, several important genes were highlighted that may potentially provide insight into the effects of liraglutide on the cardiac muscle of diabetic rats in CRC. Four modules of the PPI were chosen with most of the involved genes found to be enriched in some pathways such as glycolysis/gluconeogenesis, cardiac muscle contraction, MAPK signaling pathway, and synaptic vesicle cycle.

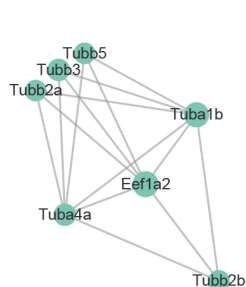
A



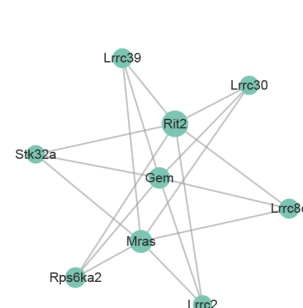
B



C



D



E

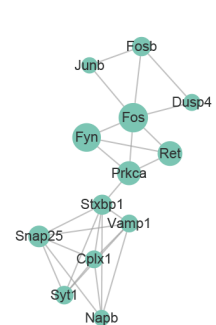


Figure 2 The protein-protein interaction (PPI) networks of DEGs and modules (A); 249 DEGs were filtered into the DEG PPI network with the STRING online database; (B) Module 1 comprises 17 nodes and 111 edges; (C) Module 2 comprises 7 nodes and 15 edges; (D) Module 3 comprises 9 nodes and 18 edges; (E) Module 4 comprises 13 nodes and 26 edges.

Table 5 The related KEGG pathways of different modules

Term	Count	Genes
Module 1		
rno04530: tight junction	4	<i>MYH1, MYH4, ACTN2, ACTN3</i>
rno04670: leukocyte transendothelial migration	3	<i>MYLPF, ACTN2, ACTN3</i>
rno04510: focal adhesion	3	<i>MYLPF, ACTN2, ACTN3</i>
rno04810: regulation of actin cytoskeleton	3	<i>MYLPF, ACTN2, ACTN3</i>
rno00010: glycolysis/gluconeogenesis	2	<i>PGAM2, ENO3</i>
rno04520: adherens junction	2	<i>ACTN2, ACTN3</i>
rno04260: cardiac muscle contraction	2	<i>MYL3, TPM2</i>
rno05410: hypertrophic cardiomyopathy (HCM)	2	<i>MYL3, TPM2</i>
rno01230: biosynthesis of amino acids	2	<i>PGAM2, ENO3</i>
Module 2		
rno04540: gap junction	6	<i>TUBB2B, TUBB2A, TUBB5, TUBA4A, TUBA1B, TUBB3</i>
rno04145: phagosome	6	<i>TUBB2B, TUBB2A, TUBB5, TUBA4A, TUBA1B, TUBB3</i>
Module 3		
rno04010: MAPK signaling pathway	2	<i>RPS6KA2, MRAS</i>
Module 4		
rno04721: synaptic vesicle cycle	4	<i>SYT1, CPLX1, STXBP1, SNAP25</i>
rno04380: osteoclast differentiation	4	<i>FOS, FYN, FOSB, JUNB</i>
rno05031: amphetamine addiction	3	<i>PRKCA, FOS, FOSB</i>
rno04725: cholinergic synapse	3	<i>PRKCA, FOS, FYN</i>
rno04010: MAPK signaling pathway	3	<i>PRKCA, DUSP4, FOS</i>
rno04664: Fc epsilon RI signaling pathway	2	<i>PRKCA, FYN</i>

GO BP term analyses revealed that up-regulated DEGs were primarily associated with muscle system processes, the development of muscle structure, and cell development, while down-regulated DEGs were associated with signal transduction and positive regulation of the immune system processes. These findings are consistent with the current theory stating that diabetic cardiomyopathy initiation and progression are highly dependent on the development of muscle structure and muscle system processes, and cell development (18). Additionally, the enriched KEGG pathways of up-regulated DEGs encompassed adrenergic signaling in cardiomyocytes and dopaminergic synapses. Previous studies have shown that adrenergic signaling in cardiomyocyte-related gene upregulation in human cardiomyocyte development wields a predictive ability of

the overall survival of cardiomyopathy patients.

PPI networks, including the top degree hub genes of Acta1, Actn2, Mapk12, Tnnc2, Actn3, Eno3, Myh1, Mylpf, Pgam2, and Pygm were also constructed. Acta1 was identified as a hub gene that regulates the non-immunosuppressive immunophilin ligand modifier of gene expression in the dorsal root ganglia during painful diabetic neuropathy (19). Reza *et al.* (20) reported that ACTA1 was a likely novel pathogenic variant in the dilated cardiomyopathy family. Tadokoro *et al.* (21) also reported that congenital myopathy demonstrated a fiber-type disproportion in the context of dilated cardiomyopathy in a patient with a novel p.G48A ACTA1 mutation. The second hub gene, Actn2, is a lone muscle isoform of α -actinin that can regulate diabetic cardiomyopathy and

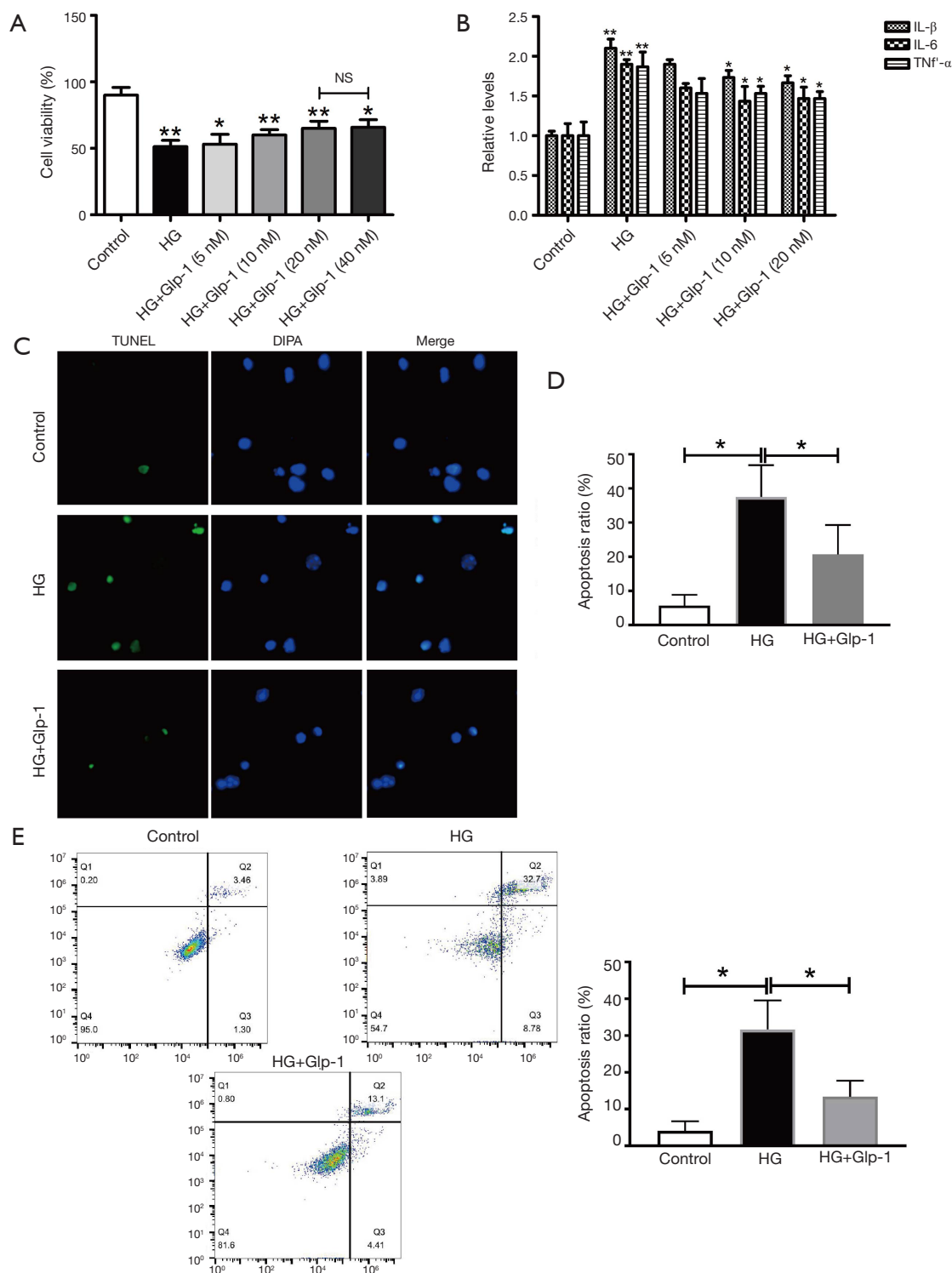


Figure 3 GLP-1 regulates H9c2 cell viability during high-glucose stress. Effects of different concentrations of GLP1 on cell viability during high-glucose Stress. (B) Effects of different concentrations of ropofol on the secretion of proinflammatory cytokines induced by high glucose in H9c2 cells. (C,D) TUNEL assay were performed to show cell apoptosis. (E) Flow cytometry were employed to show cell apoptosis. The results are shown as mean ± SEM from 5 independent experiments. *, P<0.05 and **, P<0.01 versus control. HG =22 mM high glucose. The control group was defined as 100%.

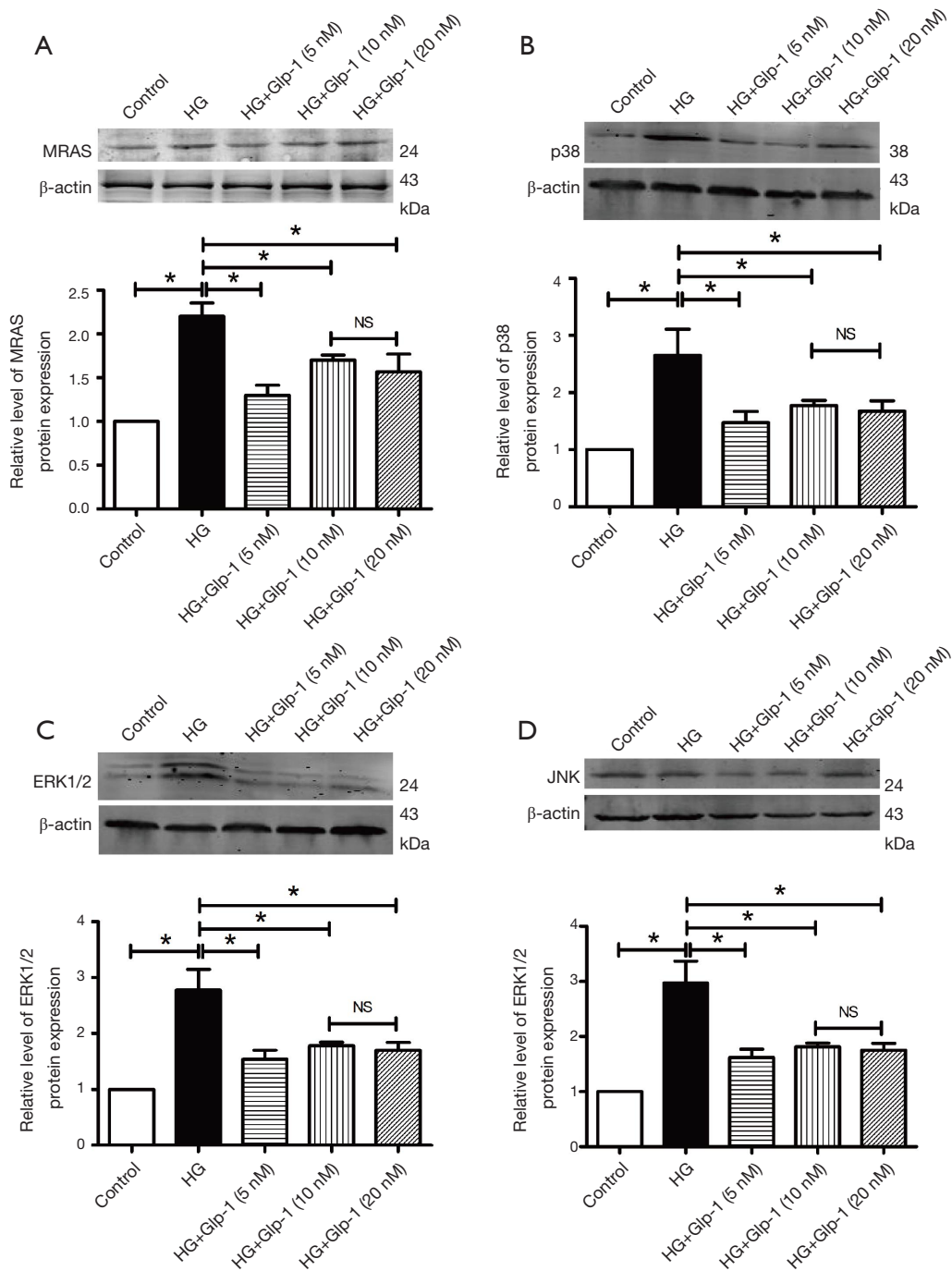


Figure 4 GLP1 decreases the expression of MRAS, p38, JNK, ERK1/2 induced by high glucose. (A,B,C,D) Expression of MRAS, p38, JNK, and ERK1/2 protein in H9c2 cells. HG with high glucose (22 mM, 72 h). n=3 for each group; *, P<0.05 versus control group or versus HG group.

is expressed abundantly on cardiac muscle (22). Previous authors have suggested that there is a relationship between diabetic cardiomyopathy and Actn2. Additionally, Actn2 affects the incorporation of cardiomyocyte Z-disc and actin-binding and therefore has a significant role in hypertrophic cardiomyopathy (22). ACTN3 is also a member of the actinin family that acts to cross proteins (23). Moreover, through *in vivo* co-immunoprecipitation, Eno3 can inhibit fluorescent 3D-co-localization in differentiated H9C2 cells (24). Myh1 has been documented to control muscle fibers, DNA repair, or tumor suppressor (25,26). Of further note, Inal-Gültekin *et al.* (27) demonstrated Pygm mutations in patients with McArdle disease in a Turkish cohort as determined by next-generation sequencing. Considering the above, additional studies investigating the function of Mylpf in diabetic cardiomyopathy are necessary (28). Nevertheless, the biological functions of Pgam2 in diabetic cardiomyopathy remain unclear.

Modular analysis of the PPI network uncovered that the effect of liraglutide on diabetic rats' cardiac muscle was associated with cardiac muscle contraction and hypertrophic cardiomyopathy (HCM). Using the STRING online database and Cytoscape software, 249 DEGs of the 520 DEGs were mapped onto a PPI network. We further analyzed the top 10 hub nodes with higher degrees. The PPI network was further assessed using MCODE plug-ins, and the top 4 modules from the PPI network were selected for the functional annotation, which played critical roles in the PPI network. Module 1 was primarily involved in tight junction, regulation of actin cytoskeleton, glycolysis/gluconeogenesis, and cardiac muscle contraction. Module 2 was primarily involved with gap junction and phagosome. Module 3 and Module 4 were primarily involved in the MAPK signaling pathway and synaptic vesicle cycle, respectively. MYL3 and TPM2 are versatile signaling molecules that regulate a diverse range of activities related to muscle growth (29). The third module/cluster consisted of the MAPK signaling pathway. These findings are backed by Higgins *et al.* who demonstrated MRAS-mediated Noonan syndrome is related to cardiac hypertrophy (30). MRAS also focuses on mineralocorticoid-receptor antagonists (31).

To investigate the role of MRAS/MAPK in glp-1-protected H9c2 cell against high-glucose injury, we first established a high-glucose injury model (32). Our data show (Figure 3) that glp-1 can inhibit H9c2 cell growth induced by high glucose. This finding is similar to that of Guan *et al.*

in whose study Glp-1 attenuated endoplasmic reticulum stress-induced apoptosis in H9c2 cardiomyocytes through GLP-1R/PI3K/Akt pathways (33). Zhang *et al.* further found that liraglutide inhibits high glucose-induced oxidative stress and apoptosis in neonatal rat cardiomyocytes (34). IL-6 (35), IL-1 β (36), and TNF- α (37) had important roles in the progress of the high glucose-induced cardiotoxicity *in vitro* model. Our data (Figure 3) indicate that glp-1 could decrease the levels of IL-6, IL-1 β , and TNF- α that were elevated by high glucose. Interestingly, glp-1 attenuated the high glucose-induced inflammation response by reducing the production of proinflammatory cytokines by inhibiting MRAS/MAPK (Figure 4).

Diabetes mellitus, a chronic metabolic disease, is becoming a significant health threat and triggers a cascade of severe, long-term complications involving the cardiovascular system, peripheral vascular system, central nervous system, and renal function. Ventricular dilatation, hypertrophy, and compromised contractile function are the major pathological manifestations of diabetic cardiomyopathy. Diabetic cardiomyopathy, which occurs independent of macro- and micro-coronary artery diseases and other cardiovascular diseases, imposes a high risk for cardiovascular morbidity and mortality. Our findings elucidated the regulatory network in diabetic cardiomyopathy and might provide a novel diagnostic and therapeutic target for diabetic cardiomyopathy.

To conclude, our study provides a comprehensive bioinformatics analysis of DEGs potentially involved in diabetic cardiomyopathy. The molecular targets uncovered in this study are prime candidates for further investigations into molecular mechanisms and biomarkers.

Acknowledgments

Funding: This work was supported in part by the National Nature Science Foundation of China (No. 81370902, 81170744).

Footnote

Conflicts of Interest: The authors have no conflicts of interest to declare.

Ethical Statement: The authors are accountable for all aspects of the work in ensuring that questions related to the accuracy or integrity of any part of the work are

appropriately investigated and resolved.

Open Access Statement: This is an Open Access article distributed in accordance with the Creative Commons Attribution-NonCommercial-NoDerivs 4.0 International License (CC BY-NC-ND 4.0), which permits the non-commercial replication and distribution of the article with the strict proviso that no changes or edits are made and the original work is properly cited (including links to both the formal publication through the relevant DOI and the license). See: <https://creativecommons.org/licenses/by-nc-nd/4.0/>.

References

- Knudsen JG, Rorsman P. beta Cell Dysfunction in Type 2 Diabetes: Drained of Energy? *Cell Metab* 2019;29:1-2.
- Dai C, Jiang S, Chu C, et al. Baicalin protects human retinal pigment epithelial cell lines against high glucose-induced cell injury by up-regulation of microRNA-145. *Exp Mol Pathol* 2019;106:123-30.
- Goedeke L, Perry RJ, Shulman GI. Emerging Pharmacological Targets for the Treatment of Nonalcoholic Fatty Liver Disease, Insulin Resistance, and Type 2 Diabetes. *Annu Rev Pharmacol Toxicol* 2019;59:65-87.
- Yao Y, Li Q, Wang W, et al. Glucagon-Like Peptide-1 Modulates Cholesterol Homeostasis by Suppressing the miR-19b-Induced Downregulation of ABCA1. *Cell Physiol Biochem* 2018;50:679-93.
- Chen X, Huang T, Shi Y, et al. A GLP1 receptor agonist attenuates human islet amyloid polypeptide-induced autophagy and apoptosis in MIN6 cells. *Mol Med Rep* 2019;19:1365-71.
- Zhang Y, Parajuli KR, Fava GE, et al. GLP-1 Receptor in Pancreatic alpha-Cells Regulates Glucagon Secretion in a Glucose-Dependent Bidirectional Manner. *Diabetes* 2019;68:34-44.
- Liu P, Song J, Liu H, et al. Insulin regulates glucagon-like peptide-1 secretion by pancreatic alpha cells. *Endocrine* 2018;62:394-403.
- Rakipovski G, Rolin B, Nohr J, et al. The GLP-1 Analogs Liraglutide and Semaglutide Reduce Atherosclerosis in ApoE(-/-) and LDLr(-/-) Mice by a Mechanism That Includes Inflammatory Pathways. *JACC Basic Transl Sci* 2018;3:844-57.
- Zhu HL, Liu ZP, Yang WY, et al. Liraglutide Ameliorates beta-Amyloid Deposits and Secondary Damage in the Ipsilateral Thalamus and Sensory Deficits After Focal Cerebral Infarction in Rats. *Front Neurosci* 2018;12:962.
- Zhang Q, Xiao X, Zheng J, et al. Liraglutide protects cardiac function in diabetic rats through the PPARalpha pathway. *Biosci Rep* 2019. [Epub ahead of print].
- Dennis G, Jr., Sherman BT, Hosack DA, et al. DAVID: Database for Annotation, Visualization, and Integrated Discovery. *Genome Biol* 2003;4:P3.
- Gene Ontology Consortium. The Gene Ontology (GO) project in 2006. *Nucleic Acids Res* 2006;34:D322-6.
- Kanehisa M, Goto S. KEGG: kyoto encyclopedia of genes and genomes. *Nucleic Acids Res* 2000;28:27-30.
- Franceschini A, Szklarczyk D, Frankild S, et al. STRING v9.1: protein-protein interaction networks, with increased coverage and integration. *Nucleic Acids Res* 2013;41:D808-15.
- Shannon P, Markiel A, Ozier O, et al. Cytoscape: a software environment for integrated models of biomolecular interaction networks. *Genome Res* 2003;13:2498-504.
- Zhao X, Huang K, Zheng M, et al. Effect of liraglutide on blood pressure: a meta-analysis of liraglutide randomized controlled trials. *BMC Endocr Disord* 2019;19:4.
- Nagaike H, Ohara M, Kohata Y, et al. Effect of Dulaglutide Versus Liraglutide on Glucose Variability, Oxidative Stress, and Endothelial Function in Type 2 Diabetes: A Prospective Study. *Diabetes Ther* 2019;10:215-28.
- Vaikhanskaya TG, Sivitskaya LN, Kurushko TV, et al. *Kardiologiya* 2018;58:33-45.
- Yamazaki S, Yamaji T, Murai N, et al. FK1706, a novel non-immunosuppressive immunophilin ligand, modifies gene expression in the dorsal root ganglia during painful diabetic neuropathy. *Neurol Res* 2012;34:469-77.
- Reza N, Garg A, Merrill SL, et al. ACTA1 Novel Likely Pathogenic Variant in a Family With Dilated Cardiomyopathy. *Circ Genom Precis Med* 2018;11:e002243.
- Tadokoro K, Ohta Y, Sasaki R, et al. Congenital myopathy with fiber-type disproportion accompanied by dilated cardiomyopathy in a patient with a novel p.G48A ACTA1 mutation. *J Neurol Sci* 2018;393:142-4.
- Haywood NJ, Wolny M, Rogers B, et al. Hypertrophic cardiomyopathy mutations in the calponin-homology domain of ACTN2 affect actin binding and cardiomyocyte Z-disc incorporation. *Biochem J* 2016;473:2485-93.
- Murphy AC, Young PW. The actinin family of actin cross-linking proteins - a genetic perspective. *Cell Biosci* 2015;5:49.

24. Uys GM, Ramburan A, Loos B, et al. Myomegalin is a novel A-kinase anchoring protein involved in the phosphorylation of cardiac myosin binding protein C. *BMC Cell Biol* 2011;12:18.
25. Ahn JS, Kim DH, Park HB, et al. Ectopic Overexpression of Porcine Myh1 Increased in Slow Muscle Fibers and Enhanced Endurance Exercise in Transgenic Mice. *Int J Mol Sci* 2018. doi: 10.3390/ijms19102959.
26. Jin J, Hwang BJ, Chang PW, et al. Interaction of apurinic/apyrimidinic endonuclease 2 (Ape2) with Myh1 DNA glycosylase in fission yeast. *DNA Repair (Amst)* 2014;15:1-10.
27. Inal-Gültekin G, Toptas-Hekimoglu B, Gormez Z, et al. Myophosphorylase (PYGM) mutations determined by next generation sequencing in a cohort from Turkey with McArdle disease. *Neuromuscul Disord* 2017;27:997-1008.
28. Ryan MT, O'Halloran AM, Hamill RM, et al. Polymorphisms in the regulatory region of the porcine MYLPF gene are related to meat quality traits in the Large White breed. *Meat Sci* 2016;113:104-6.
29. Wang Z, Shang P, Li Q, et al. iTRAQ-based proteomic analysis reveals key proteins affecting muscle growth and lipid deposition in pigs. *Sci Rep* 2017;7:46717.
30. Higgins EM, Bos JM, Mason-Suares H, et al. Elucidation of MRAS-mediated Noonan syndrome with cardiac hypertrophy. *JCI Insight* 2017;2:e91225.
31. Yugar-Toledo JC, Modolo R, de Faria AP, et al. Managing resistant hypertension: focus on mineralocorticoid-receptor antagonists. *Vasc Health Risk Manag* 2017;13:403-11.
32. Yang M, Lin Y, Wang Y, et al. High-glucose induces cardiac myocytes apoptosis through Foxo1/GRK2 signaling pathway. *Biochem Biophys Res Commun* 2019;513:154-8.
33. Guan G, Zhang J, Liu S, et al. Glucagon-like peptide-1 attenuates endoplasmic reticulum stress-induced apoptosis in H9c2 cardiomyocytes during hypoxia/reoxygenation through the GLP-1R/PI3K/Akt pathways. *Naunyn Schmiedebergs Arch Pharmacol* 2019;392:715-22.
34. Zhang L, Li C, Zhu Q, et al. Liraglutide, a glucagon-like peptide-1 analog, inhibits high glucose-induced oxidative stress and apoptosis in neonatal rat cardiomyocytes. *Exp Ther Med* 2019;17:3734-40.
35. Ye EA, Steinle JJ. miR-146a suppresses STAT3/VEGF pathways and reduces apoptosis through IL-6 signaling in primary human retinal microvascular endothelial cells in high glucose conditions. *Vision Res* 2017;139:15-22.
36. Hu L, Yang H, Ai M, et al. Inhibition of TLR4 alleviates the inflammation and apoptosis of retinal ganglion cells in high glucose. *Graefes Arch Clin Exp Ophthalmol* 2017;255:2199-210.
37. Sun M, Yang J, Wang J, et al. TNF-alpha is upregulated in T2DM patients with fracture and promotes the apoptosis of osteoblast cells in vitro in the presence of high glucose. *Cytokine* 2016;80:35-42.

Cite this article as: Dong Y, Yan S, Li GY, Wang MN, Leng L, Li Q. Identification of key candidate genes and pathways revealing the protective effect of liraglutide on diabetic cardiac muscle by integrated bioinformatics analysis. *Ann Transl Med* 2020;8(5):181. doi: 10.21037/atm.2020.01.94

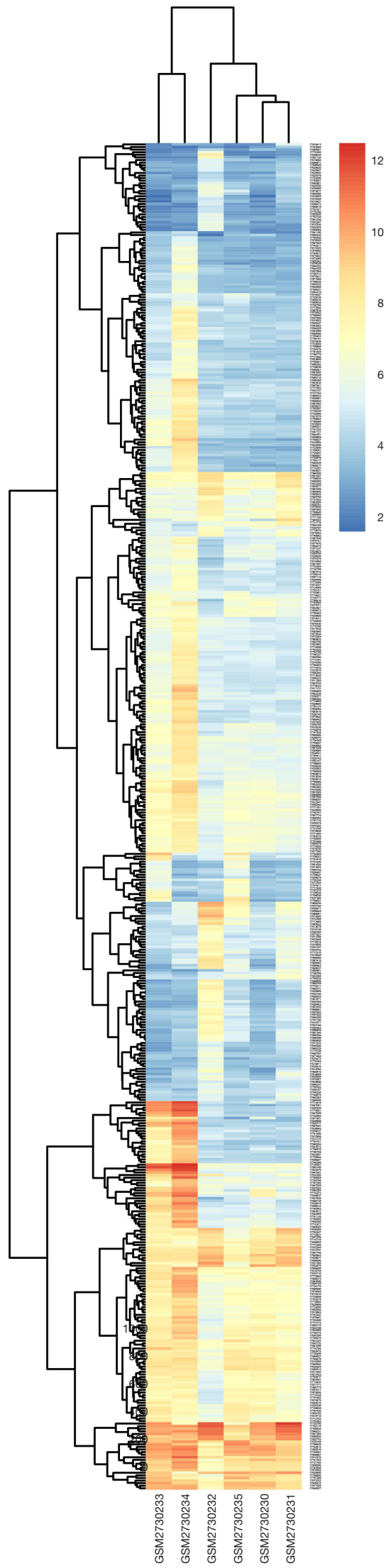


Figure S1 Heat map of the 520 DEGs using the GSE102194 data profile.

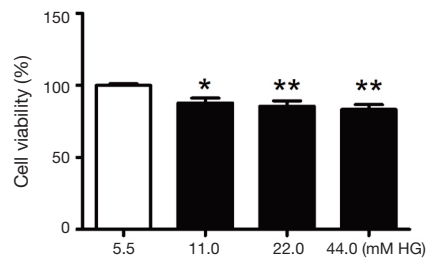


Figure S2 Different concentrations (5.5, 11, 22, and 44 mM) of glucose inhibiting H9c2 cell viability by CCK-8. *P<0.05, **P<0.01 versus control group or versus HG group.